Metal-Oxide-Free Methylammonium Lead Iodide Perovskite-Based Solar Cells: the Influence of Organic Charge Transport Layers

ARTICLE *in* ADVANCED ENERGY MATERIALS · OCTOBER 2014

Impact Factor: 16.15 · DOI: 10.1002/aenm.201400345

7 AUTHORS, INCLUDING:

Alejandra Soriano-Portillo
University of Valencia
25 PUBLICATIONS **590** CITATIONS
SEE PROFILE

Enrico Bandiello
University of Valencia
10 PUBLICATIONS **93** CITATIONS
SEE PROFILE

Md Khaja Nazeeruddin
École Polytechnique Fédérale de Lausanne
489 PUBLICATIONS **44,979** CITATIONS
SEE PROFILE

Henk J. Bolink
University of Valencia
208 PUBLICATIONS **4,905** CITATIONS
SEE PROFILE

LETTERS
PUBLISHED ONLINE: 22 DECEMBER 2013 | DOI: 10.1038/NPHOTON.2013.341
nature photonics

Perovskite solar cells employing organic charge-transport layers

Olga Malinkiewicz[1], Aswani Yella[2], Yong Hui Lee[2], Guillermo Mínguez Espallargas[1], Michael Graetzel[2], Mohammad K. Nazeeruddin[2]* and Henk J. Bolink[1]*

Thin-film photovoltaics play an important role in the quest for clean renewable energy. Recently, methylammonium lead halide perovskites were identified as promising absorbers for solar cells[1]. In the three years since, the performance of perovskite-based solar cells has improved rapidly to reach efficiencies as high as 15%[1–10]. To date, all high-efficiency perovskite solar cells reported make use of a (mesoscopic) metal oxide, such as Al_2O_3, TiO_2 or ZrO_2, which requires a high-temperature sintering process. Here, we show that methylammonium lead iodide perovskite layers, when sandwiched between two thin organic charge-transporting layers, also lead to solar cells with high power-conversion efficiencies (12%). To ensure a high purity, the perovskite layers were prepared by sublimation in a high-vacuum chamber. This simple planar device structure and the room-temperature deposition processes are suitable for many conducting substrates, including plastic and textiles.

The hybrid organic–inorganic methylammonium lead halide perovskites, pioneered by Mitzi, are recognized for their excellent semiconducting properties[11,12]. Following the pioneering work of Miyasaka and co-workers[1], the ease with which these organic–inorganic hybrid perovskite materials can be prepared and processed from solution makes them attractive for photovoltaic applications[13]. In their studies, the methylammonium lead iodide perovskite was used as a sensitizer in liquid dye-sensitized solar cells and an efficiency of 3.8% was obtained. The low efficiency results from the solubility of the perovskite layer in the iodine/iodide redox electrolyte system. High efficiencies have been realized by replacing the liquid electrolyte with a solid hole-transporting material such as 2,2′,7,7′-tetrakis(*N*,*N*-di-*p*-methoxyphenylamine)-9,9′-spirobifluorene (spiro-MeOTAD), as reported by the groups of Snaith and Graetzel[2–9]. Interestingly, Lee *et al.*[6] showed that a mixed-halide perovskite on a mesoporous Al_2O_3 photoanode acts both as a light absorber and an electron conductor. Etgar *et al.*[8] reported that the pure methylammonium lead iodide perovskite also acts as an efficient hole conductor. Recently, Burschka *et al.*[4] published a high power-conversion efficiency of 15% for a solar cell in which the perovskite was deposited by a novel sequential deposition technique on a mesoporous TiO_2 film. Ball *et al.*[5] showed that a thick layer (350 nm) of the mixed-halide methylammonium lead perovskite ($CH_3NH_3PbI_{3-x}Cl_x$) leads to efficient solar cells (12%). They argue that the perovskite functions as the absorber and as the electron and hole transporter. Additionally, it was suggested that the excitons dissociate predominantly in the bulk and not at a donor–acceptor interface. The operating mechanism of planar perovskite solar cells, however, is not clear. For example, it was shown that the photoluminescence of a mixed-halide methylammonium lead perovskite was reduced strongly when either a hole- or an electron-transporting layer was deposited on top of it[14]. A similar effect, but less strong, was observed for thin films of the pure iodide methylammonium lead perovskite[14]. Hence, exciton dissociation may occur both in the bulk and at the perovskite interface. Currently, the dominant process is not established and may well depend on the exact nature of the perovskite film. Up to now, the highest efficiency was reported by Liu *et al.*, who used a thin metal oxide layer and a sublimed perovskite layer that leads to solar cells with an efficiency of 15.4%[9]. High material purity is essential for efficient charge-carrier transport and to prevent exciton quenching, as established in organic light-emitting diodes and organic photovoltaic (OPV) devices[15,16]. Therefore, in these devices vacuum sublimation is employed frequently to achieve high-purity layers. Solution-processed perovskites are generated *in situ* and therefore may contain imperfections and impurities. Purification of the perovskite layer is not possible as it decomposes on dissolving.

An inverted layout, similar to that employed in small molecular weight and polymeric solar cells, has also been described[17,18]. In these bilayer planar heterojunction devices, the perovskite layer was used as the electron donor in combination with an electron acceptor, in analogy to a frequently used OPV layout. The holes are extracted via the transparent conductor poly(3,4-ethylenedioxythiophene):poly(styrenesulfonic acid) (PEDOT:PSS). The device performances, however, were significantly inferior to those of devices that employ (mesoporous) metal oxides.

Here, we present an inverted thin-film solar cell based on a sublimed methylammonium lead iodide perovskite layer sandwiched between two very thin electron- and hole-blocking layers that consist of organic molecules. The organic materials were deposited using solution-based processes, whereas the $CH_3NH_3PbI_3$ perovskite and the metal contact were deposited using thermal evaporation under vacuum. These simple devices, free of metal oxide and prepared using room-temperature processing, reach efficiencies as high as 12% at 100 mW cm^{-2}, which demonstrate their potential for a wide variety of photovoltaic applications.

The $CH_3NH_3PbI_3$ perovskite thin film was prepared by coevaporation of the two starting compounds, CH_3NH_3I and PbI_2. Details of the experimental conditions are given in the Methods section. These films were characterized using grazing incidence X-ray diffraction (GIXRD). Initially, excess PbI_2 was present in the film, yet on optimizing the evaporation process, highly oriented pure $CH_3NH_3PbI_3$ films were obtained (see Fig 1a and Supplementary Fig. 1). The films adopt the typical tetragonal structure for $CH_3NH_3MX_3$ hybrid perovskites (M = Pb, Sn; X = Cl, Br, I) formed by a three-dimensional anionic framework of PbI_6 octahedra with the methylammonium cations in the interstitial space (see Fig. 1b)[19]. The roughness of the $CH_3NH_3PbI_3$ film was evaluated using atomic force microscopy (AFM) and an image of a typical

[1]Instituto de Ciencia Molecular, Universidad de Valencia, C/Catedrático J. Beltrán 2, 46980 Paterna (Valencia), Spain, [2]Laboratory of Photonics and Interfaces, Swiss Federal Institute of Technology (EPFL), Station 6, Lausanne, CH 1015, Switzerland. *e-mail: mdkhaja.nazeeruddin@epfl.ch; henk.bolink@uv.es

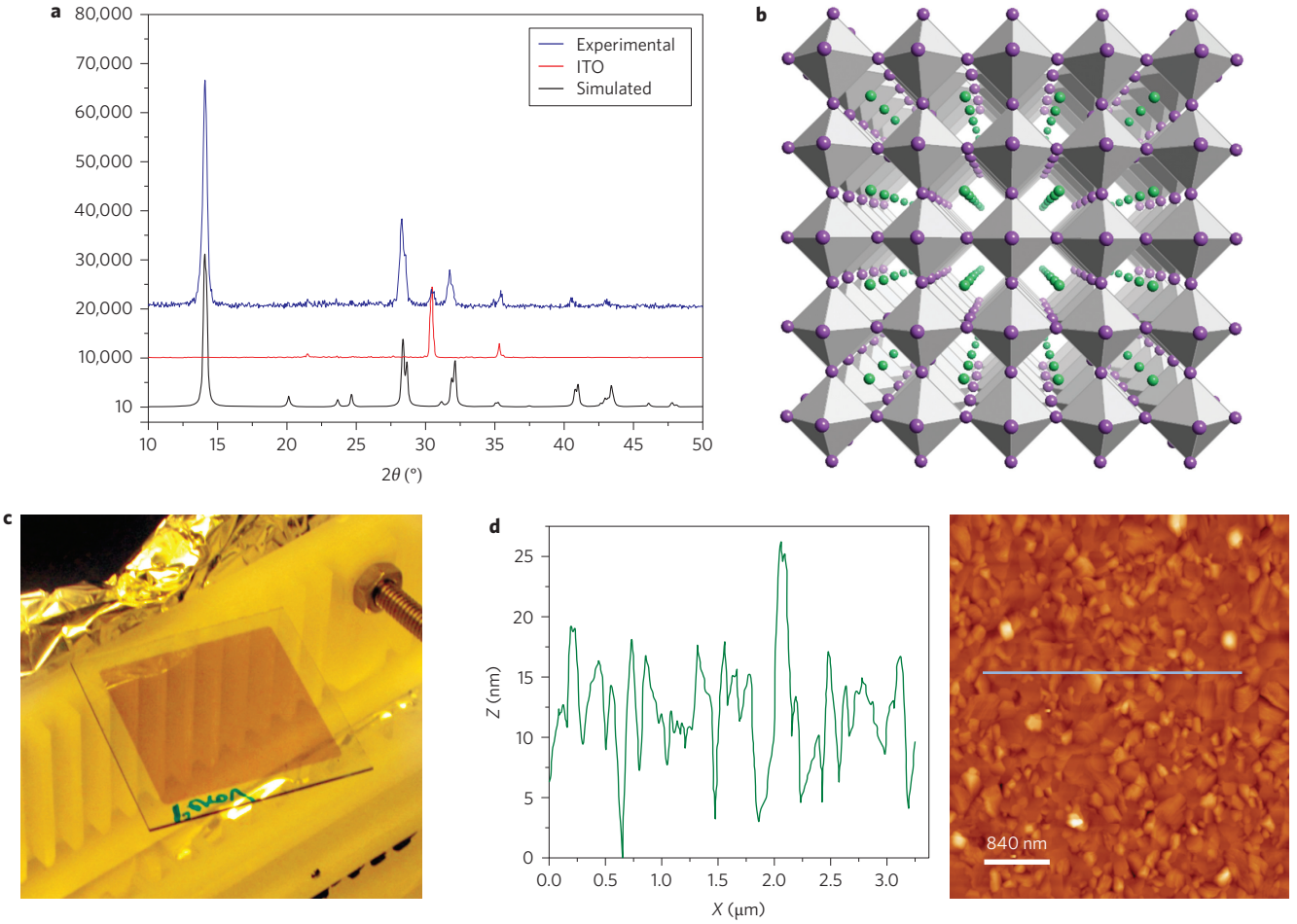

Figure 1 | Characteristics of the sublimed $CH_3NH_3PbI_3$ perovskite layer. a, GIXRD pattern with Cu $K\alpha_1$ radiation ($\lambda = 1.54056$ Å) of the sublimed thin film (blue), ITO substrate (red) and calculated for $CH_3NH_3PbI_3$ with preferred orientation along the (100) and (001) directions. **b**, Simulation of the crystal structure of $CH_3NH_3PbI_3$ perovskite. Pb atoms are placed at the centre of the grey octahedrons, lavender spheres represent iodine atoms and green spheres represent the methylammonium cations. **c**, Photograph of a 20-nm-thick film. **d**, AFM image and profile of a 60-nm-thick film.

scan is given in Fig. 1d, which demonstrates a smooth film with a root mean square roughness of 5 nm. Figure 1c is a photograph of a 20-nm-thick film.

As the $CH_3NH_3PbI_3$ layer is prepared via vacuum sublimation, it can be implemented easily in different device architectures. To demonstrate that the $CH_3NH_3PbI_3$ is capable of performing most of the roles required to obtain an efficient solar cell and to minimize the use of costly organic semiconductors, a simple device structure was chosen. In this structure, which is typical for both organic photovoltaic and light-emitting devices, a semitransparent organic conductor was used as the positive charge-collecting contact. The structure of the device is shown in Fig. 2a, and consists of a 70 nm PEDOT:PSS layer and a thin layer (<10 nm) of poly(*N*,*N*′-bis(4-butylphenyl)-*N*,*N*′-bis(phenyl)benzidine) (polyTPD) (Fig. 2c) as the electron-blocking layer. On top of this, the $CH_3NH_3PbI_3$ was evaporated thermally to a thickness of 285 nm followed by a thin layer (<10 nm) of (6,6)-phenyl C_{61}-butyric acid methyl ester (PCBM) as the hole-blocking layer (Fig. 2d)[20]. The device was completed by the evaporation of an Au top electrode (100 nm). Both the polyTPD and the PCBM layers were deposited using a meniscus-coating process to ensure high-quality films[21]. The thickness of the layers was established using absorbance measurements.

The relevant energy levels of the materials used to prepare the solar cell are depicted in Fig. 2b. The valence band (VB) and conduction band (CB) of the $CH_3NH_3PbI_3$ perovskite are −5.4 and −3.9 eV, versus vacuum, respectively[7]. On illuminating the device, excitons are generated in the $CH_3NH_3PbI_3$ perovskite layer. It was reported that excitons in $CH_3NH_3PbI_3$ perovskites are of the Wannier–Mott type, which implies that they may dissociate in the bulk of the perovskite layer[5,12]. Owing to the use of indium–tin oxide (ITO)/PEDOT:PSS as the hole-collecting contact and Au as the electron-collecting electrode, the built-in voltage of this device is small. Hence, to direct the flow of electrons and holes, thin hole-blocking and electron-blocking layers are incorporated adjacent to the perovskite layer. PolyTPD and PCBM were selected for this role as their highest occupied molecular orbital (HOMO) and lowest unoccupied molecular orbital (LUMO) levels, respectively, match well with the VB and CB of the perovskite, which allows for a good transport of holes towards the polyTPD and of electrons to the PCBM layer (Fig. 2b). As the LUMO of polyTPD is significantly closer to vacuum compared with that of the perovskite CB, polyTPD efficiently blocks the flow of electrons. The opposite process, the blocking of holes, occurs at the perovskite–PCBM interface because of the lower HOMO of PCBM compared with that of the perovskite VB. As mentioned above, exciton dissociation may also occur at the perovskite–polyTPD and perovskite–PCBM interfaces[14].

Figure 3a shows the current–voltage (J–V) characteristics of a typical small-area (0.09 cm^2) perovskite solar cell measured in the dark and under light intensities of 100, 50 and 10 mW cm^{-2}. The

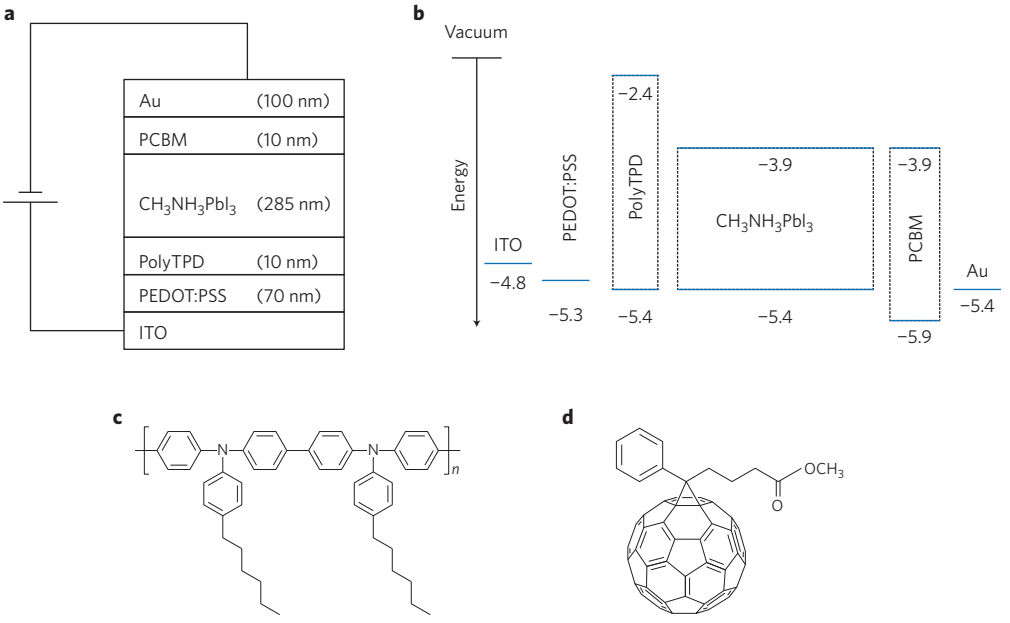

Figure 2 | Schematics of the device. a, Stacked layer structure. **b**, Schematic of the relative energy levels of each layer. **c**, Chemical structure of the polyarylamine (polyTPD). **d**, Chemical structure of PCBM.

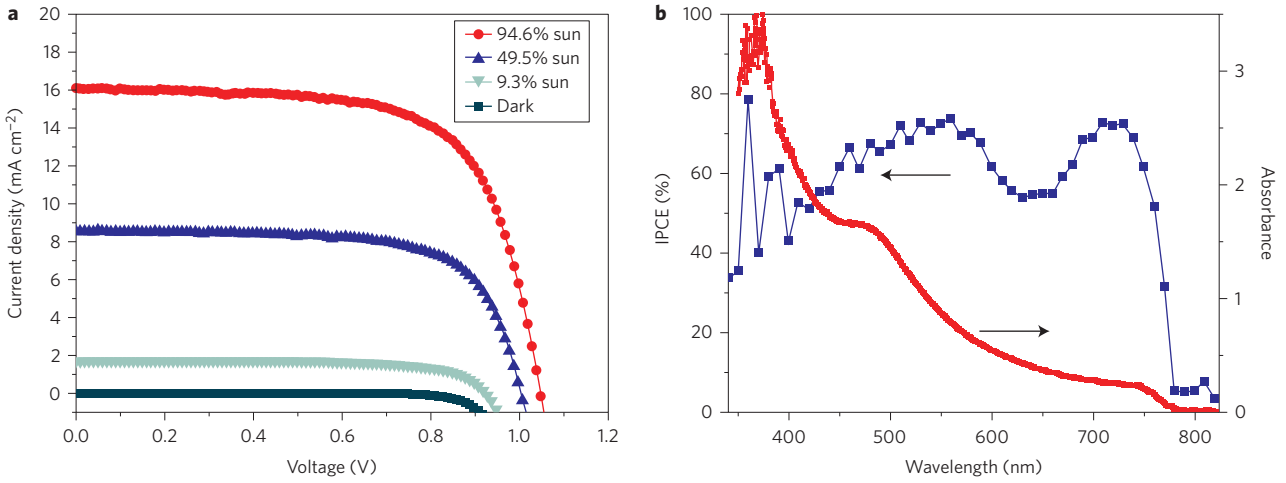

Figure 3 | Typical *J–V* and IPCE characteristics of the perovskite solar cell. a, Photocurrent density versus voltage at 100, 50 and 10 mW cm^{-2} and in the dark. **b**, IPCE spectrum and absorbance of a 285-nm-thick perovskite layer.

reproducibility from device to device was excellent, with less than 10% deviation. The short-circuit current density (J_{SC}), open-circuit voltage (V_{OC}) and fill factor (*FF*), respectively, are 16.12 mA cm^{-2}, 1.05 V and 0.67, which lead to a power-conversion efficiency of 12.04% measured at 100 mW cm^{-2}. At 50 and 10 mW cm^{-2} the device exhibited very similar efficiencies, 12.04% and 12.00%, respectively. The high open-circuit potential indicates that there are negligible surface and sub-bandgap states in the perovskite film. The device performance under 100 mW cm^{-2} is remarkable in view of the very thin perovskite film of 285 nm. A device with cells of larger area (0.98 cm^2) was also prepared and evaluated at 100 mW cm^{-2} (Supplementary Fig. 4). The J_{SC} and V_{OC} are very similar to the data obtained for the small-area cell (14.76 mA cm^{-2} and 1.05 V, respectively). The *FF*, however, is significantly lower (0.52), which is the main reason for the lower power-conversion efficiency (8.27%) for these larger cells.

The incident photon-to-current conversion efficiency (IPCE) spectra exhibit 74% (Fig. 3b) where the generation of photocurrent started at 790 nm, in agreement with the bandgap of the $CH_3NH_3PbI_3$. It is interesting that the IPCE spectra show a very steep onset, contrary to the IPCE spectra reported for TiO_2 and Al_2O_3 mesoscopic-based perovskite cells. A very similar IPCE spectrum as observed for our solar cells was reported for a solar cell based on a perovskite layer sandwiched between a C_{60}-modified TiO_2 layer and a layer of poly(3-hexylthiophene)[22]. As such, the steep onset may be related to the specific interaction of the perovskite with the fullerene molecules. The IPCE spectrum is almost flat, except for a dip at 630 nm that could result from the oxidized polyTPD acting as a filter or from reduced absorption of the perovskite. Integrating the overlap of the IPCE spectrum with the AM1.5G solar photon flux yields a current density of 16.40 mA cm^{-2}, which is in excellent agreement with the measured photocurrent density of

16.12 mA cm^{-2} at the standard solar AM1.5G intensity of 100 mW cm^{-2}, which confirms that the mismatch between the simulated sunlight and the AM1.5G standard is negligible. The absorbance of the $CH_3NH_3PbI_3$ film is similar to those reported previously for this material and increases with increasing layer thickness (Fig. 3b). The absorption extends over the complete visible spectrum up to 800 nm, with a local maximum around 500 nm (the scale of the graph in Fig. 3b is optical density).

Conclusion

An efficient solid-state, thin-film solar cell was obtained by sandwiching a sublimated $CH_3NH_3PbI_3$ perovskite layer between two thin organic charge-transporting layers that function as hole and electron blockers, respectively, and contacting it via an indium tin oxide (ITO)/PEDOT:PSS as the hole-extraction and an Au electron-extraction contact. The simple device architecture, which is an *n*-type oxide and scaffold free, coupled with easy room-temperature fabrication using economically favourable materials, high efficiency and high reproducibility rivals strongly the established thin-film photovoltaic technologies. The device power-conversion efficiency of 12% at 100 mW cm^{-2} is remarkable in view of the very thin (285 nm) perovskite film. The high J_{sc} of 16.12 mA cm^{-2} and the open-circuit potential of 1.05 V reveal that very few electrons and holes recombine, which demonstrates the effectiveness of the hole- and electron-blocking layers. We believe that this new class of perovskite solar cell using organic semiconductors to collect the charges will find widespread applications to rival photovoltaic solar cells based on thin films.

Note added in proof: During the revision of this paper, a highly relevant article to this topic was published: P. Docampo, J.M. Ball, M. Darwich, G.E. Eperon & H.J. Snaith, Efficient organometal trihalide perovskite planar-heterojunction solar cells on flexible polymer substrates. *Nature Commun.* **4**, 2761 (2013).

Methods

Materials. Photolithographically patterned ITO-covered glass substrates were purchased from NaranjoSubstrates. Aqueous dispersions of PEDOT:PSS (Clevios P VP Al 4083) were obtained from Heraeus Holding and used as received. Poly-TPD was purchased from ADS Dyesource. PbI_2 was purchased from Aldrich and used as is. CH_3NH_3I was prepared similarly to a previously published method[8]; in brief, CH_3NH_3I was synthesized by reacting 21.6 ml methylamine (40 wt% in water; Aldrich) and 30 ml hydroiodic acid (57 wt% in water; Aldrich) in a 250 ml round-bottomed flask at 0 °C for 2 h with stirring. The white precipitate was recovered by evaporation at 50 °C for 1 h. The product, CH_3NH_3I, was dissolved in ethanol, filtered, recrystallized from diethyl ether and dried at 60 °C in a vacuum oven for 24 h.

Device preparation. Devices were prepared on cleaned ITO substrates by spin coating a thin layer of PEDOT:PSS from the commercial aqueous dispersion (1,200 revolutions per minute for 30 s (Chemmat, 3 cm diameter), which resulted in a thickness of 70 nm). On top of this layer a thin film of polyTPD was deposited from a chlorobenzene solution (10 mg ml^{-1}) using a meniscus coater and a coating speed of 2.5 mm s^{-1}. Then the substrates were transferred to a vacuum chamber integrated into an inert glovebox (<0.1 ppm O_2 and <0.1 ppm H_2O; MBraun) and evacuated to a pressure of 1×10^{-6} mbar. Two ceramic crucibles were filled with CH_3NH_3I (freshly prepared) and PbI_2, which were heated to 70 °C and 250 °C, respectively. The film thickness was controlled by the PbI_2 evaporation at a rate of evaporation of 0.5 Å s^{-1} (see Supplementary Information for more details concerning the perovskite evaporation process). The PCBM layer was deposited using a chlorobenzene solution (10 mg ml^{-1}) in ambient conditions with a meniscus coater and a coating speed of 10 mm s^{-1}. The device was completed by the thermal evaporation of the top metal electrode under a base pressure of 2×10^{-6} mbar to a thickness of 100 nm. The solar cells (active area of 0.09 and 0.98 cm^2) were then encapsulated with a glass cover using an ultraviolet-curable epoxy sealant (Ossila E131 Encapsulation Epoxy), with an ultraviolet exposure of 5 min.

Characterization. GIXRD data were collected at room temperature in the 2θ range 5–50° on an Empyrean PANalytical powder diffractometer using Cu $K\alpha_1$ radiation. Typically, four repeated measurements were collected and merged into a single diffractogram. Pawley refinements[23] were performed using the TOPAS computer program[24] and revealed an excellent fit to a one-phase model with a tetragonal cell ($a = 8.80(2)$, $c = 12.57(2)$ Å) and space group *I*4/*mcm*. Additional peaks that correspond to the ITO substrate were also observed. The observed and calculated diffraction patterns for the refined crystal structures are shown in Supplementary Fig. 3.

Simulation of the crystal structure of $CH_3NH_3PbI_3$ perovskite was performed using, as a starting model, the isostructural Sn analogue (CCDC ref. code: ZZZBWS02), and modifying the cell parameters to those obtained in the Pawley refinement[25].

Absorption spectra were taken using a fibre-optics based Aventes Avaspec2048 spectrometer.

Current–voltage characteristics were recorded by applying an external potential bias to the cell and recording the generated photocurrent with a digital source meter (Keithley Model 2400). The light source was a 450 W xenon lamp (Oriel) equipped with a Schott K113 Tempax sunlight filter (Praezisions Glas & Optik) to match the emission spectrum of the lamp to the AM1.5G standard. A black mask was used in the photovoltaic studies to limit the active area of the device. Before each measurement, the exact light intensity was determined using a calibrated Si reference diode equipped with an infrared cut-off filter (KG-3, Schott). IPCE measurements were determined using a 300 W xenon light source (ILC Technology). A Gemini-180 double monochromator (Jobin Yvon) was used to select and increment the wavelength of the radiation that impinged on the cells. The monochromatic incident light was passed through a chopper run at 1 Hz frequency, and the on/off ratio was measured by an operational amplifier. IPCE spectra were recorded as functions of wavelength under a constant white-light bias of approximately 5 mW cm^{-2} supplied by an array of diodes that emitted white light. The excitation beam from a 300 W xenon lamp (ILC Technology) was focused through a Gemini-180 double monochromator (Jobin Yvon) and chopped at approximately 2 Hz. The signal was recorded using a Model SR830 DSP Lock-In Amplifier (Stanford Research Systems).

Received 16 September 2013; accepted 14 November 2013; published online 22 December 2013

References

1. Kojima, A., Teshima, K., Shirai, Y. & Miyasaka, T. Organometal halide perovskites as visible-light sensitizers for photovoltaic cells. *J. Am. Chem. Soc.* **131,** 6050–6051 (2009).
2. Kim, H.-S. *et al.* High efficiency solid-state sensitized solar cell-based on submicrometer rutile TiO_2 nanorod and $CH_3NH_3PbI_3$ perovskite sensitizer. *Nano Lett.* **13,** 2412–2417 (2013).
3. Heo, J. H. *et al.* Efficient inorganic–organic hybrid heterojunction solar cells containing perovskite compound and polymeric hole conductors. *Nature Photon.* **7,** 486–491 (2013).
4. Burschka, J. *et al.* Sequential deposition as a route to high-performance perovskite-sensitized solar cells. *Nature* **499,** 316–319 (2013).
5. Ball, J. M., Lee, M. M., Hey, A. & Snaith, H. J. Low-temperature processed meso-superstructured to thin-film perovskite solar cells. *Energy Environ. Sci.* **6,** 1739–1743 (2013).
6. Lee, M. M., Teuscher, J., Miyasaka, T., Murakami, T. N. & Snaith, H. J. Efficient hybrid solar cells based on meso-superstructured organometal halide perovskites. *Science* **338,** 643–647 (2012).
7. Kim, H-S. *et al.* Lead iodide perovskite sensitized all-solid-state submicron thin film mesoscopic solar cell with efficiency exceeding 9%. *Sci. Rep.* **2,** 591 (2012).
8. Etgar, L. *et al.* Mesoscopic $CH_3NH_3PbI_3/TiO_2$ heterojunction solar cells. *J. Am. Chem. Soc.* **134,** 17396–17399 (2012).
9. Liu, M., Johnston, M. B. & Snaith, H. J. Efficient planar heterojunction perovskite solar cells by vapour deposition. *Nature* **501,** 395–398 (2013).
10. Hodes, G. Perovskite-based solar cells. *Science* **342,** 317–318 (2013).
11. Kagan, C. R., Mitzi, D. B. & Dimitrakopoulos, C. D. Organic–inorganic hybrid materials as semiconducting channels in thin-film field-effect transistors. *Science* **286,** 945–947 (1999).
12. Tanaka, K. *et al.* Comparative study on the excitons in lead-halide-based perovskite-type crystals $CH_3NH_3PbBr_3$ and $CH_3NH_3PbI_3$. *Solid State Commun.* **127,** 619–623 (2003).
13. Snaith, H. J. Perovskites: the emergence of a new era for low-cost, high-efficiency solar cells. *J. Phys. Chem. Lett.* **4,** 3623–3630 (2013).
14. Stranks, S. D. *et al.* Electron-hole diffusion lengths exceeding 1 micrometer in an organometal trihalide perovskite absorber. *Science* **342,** 341–344 (2013).
15. Sasabe, H. & Kido, J. Development of high performance OLEDs for general lighting. *J. Mater. Chem. C* **1,** 1699–1707 (2013).
16. Riede, M., Mueller, T., Tress, W., Schueppel, R. & Leo, K. Small-molecule solar cells—status and perspectives. *Nanotechnology* **19,** 424001 (2008).
17. Jeng, J-Y. *et al.* $CH_3NH_3PbI_3$ perovskite/fullerene planar-heterojunction hybrid solar cells. *Adv. Mater.* **25,** 3727–3732 (2013).
18. Sun, S. *et al.* The origin of high efficiency in low-temperature solution-processable bilayer organometal halide hybrid solar cells. *Energy Environ. Sci.* http://dx.doi.org/10.1039/C3EE43161D (2014).
19. Mitzi, D. B. in *Progress in Inorganic Chemistry*, Vol. 48 (ed. Karin, K.D.) 1–121 (John Wiley, 2007).
20. Yu, G., Gao, J., Hummelen, J. C., Wudl, F. & Heeger, A. J. Polymer photovoltaic cells: enhanced efficiencies via a network of internal donor–acceptor heterojunctions. *Science* **270,** 1789–1791 (1995).

21. Malinkiewicz, O., Lenes, M., Brine, H. & Bolink, H. J. Meniscus coated high open-circuit voltage bi-layer solar cells. *RSC Adv.* **2,** 3335–3339 (2012).
22. Abrusci, A. *et al.* High-performance perovskite–polymer hybrid solar cells via electronic coupling with fullerene monolayers. *Nano Lett.* **13,** 3124–3128 (2013).
23. Pawley, G. S. Unit-cell refinement from powder diffraction scans. *J. Appl. Cryst.* **14,** 357–361 (1981).
24. TOPAS-Academic, Version 4.1, 2007, http://www.topas-academic.net (Coelho Software, Brisbane).
25. Takahashi, Y. *et al.* Charge-transport in tin-iodide perovskite $CH_3NH_3SnI_3$: origin of high conductivity. *Dalton Trans.* **40,** 5563–5568 (2011).

Acknowledgements

We thank A. Soriano-Portillo, J. Ferrando, A. K. Chandiran and E. Ortí for their assistance with the sample preparation and characterization, and careful proofreading of the manuscript. This work was supported by the European Community's Seventh Framework Programme (ORION, Grant 229036 and NANOMATCELL, Grant 308997), the Spanish Ministry of Economy and Competitiveness (MAT2011-24594), the Generalitat Valenciana (Prometeo/2012/053) and the Global Research Laboratory Program, Korea (GLOBASOL, Grant 309194).

Author contributions

O.M. designed, prepared and characterized the devices, A.Y. and Y.H.L. characterized the devices, G.M.E. supervised the X-ray characterization and interpretation, M.G. supervised the work and wrote the manuscript, M.K.N. initiated the research, provided key materials and wrote the manuscript, H.J.B initiated the research, designed the devices, supervised the work and wrote the manuscript.

Additional information

Supplementary information is available in the online version of the paper. Reprints and permissions information is available online at www.nature.com/reprints. Correspondence and requests for materials should be addressed to M.K.N. and H.J.B.

Competing financial interests

The authors declare no competing financial interests.